Hindawi Publishing Corporation
EURASIP Journal on Wireless Communications and Networking
Volume 2007, Article ID 29086, 12 pages
doi:10.1155/2007/29086

Research Article

Burst Format Design for Optimum Joint Estimation of Doppler-Shift and Doppler-Rate in Packet Satellite Communications

Luca Giugno,[1] Francesca Zanier,[2] and Marco Luise[2]

[1] *Wiser S.r.l.–Wireless Systems Engineering and Research, Via Fiume 23, 57123 Livorno, Italy*
[2] *Dipartimento di Ingegneria dell'Informazione, University of Pisa, Via Caruso 16, 56122 Pisa, Italy*

Received 1 September 2006; Accepted 10 February 2007

Recommended by Anton Donner

This paper considers the problem of optimizing the burst format of packet transmission to perform enhanced-accuracy estimation of Doppler-shift and Doppler-rate of the carrier of the received signal, due to relative motion between the transmitter and the receiver. Two novel burst formats that minimize the Doppler-shift and the Doppler-rate Cramér-Rao bounds (*CRB*s) for the joint estimation of carrier phase/Doppler-shift and of the Doppler-rate are derived, and a data-aided (DA) estimation algorithm suitable for each optimal burst format is presented. Performance of the newly derived estimators is evaluated by analysis and by simulation, showing that such algorithms attain their relevant *CRB*s with very low complexity, so that they can be directly embedded into new-generation digital modems for satellite communications at low SNR.

1. INTRODUCTION

Packet transmission of digital data is nowadays adopted in several wireless communications systems such as satellite time-division multiple access (TDMA) and terrestrial mobile cellular radio. In those scenarios, the received signal may suffer from significant time-varying Doppler distortion due to relative motion between the transmitter and the receiver. This occurs, for instance, in the last-generation mobile-satellite communication systems based on a constellation of nongeostationary low-earth-orbit (LEO) satellites [1] and in millimeter-wave mobile communications for traffic control and assistance [2]. In such situations, carrier Doppler-shift and Doppler-rate estimation must be performed at the receiver for correct demodulation of the received signal.

A number of efficient digital signal processing (DSP) algorithms have already been developed for the estimation of the Doppler-shift affecting the received carrier [3] and a few algorithms for Doppler-rate estimation are also available in the open literature [4, 5]. The issue of *joint* Doppler-shift *and* Doppler-rate estimation has been addressed as well, although to a lesser extent [6, 7]. In all the papers above, the observed signal is either an unmodulated carrier, or contains pilot symbols known at the receiver. The most common burst format is the conventional *preamble-payload* arrangement, wherein all pilots are consecutive and they are placed at the beginning of the data burst. Other formats are the *midamble* as in the GSM system [8], wherein the preamble is moved to the center of the burst, or the so-called pilot symbol assisted modulation (PSAM) paradigm [9], where the set of pilot symbols is regularly multiplexed with data symbols in a given ratio (the so-called burst overhead). Data-aided (DA) algorithms, which exploit the information contained in the pilot symbols, are routinely used to attain good performance with small burst overhead. The recent introduction of efficient channel coding with iterative detection [10] has also placed new and more stringent requirements for receiver synchronization on satellite modems. The carrier synchronizer is requested to operate at a lower signal-to-noise ratio (SNR) than it used to be with conventional coding [11].

Therefore, it makes sense to search for the ultimate accuracy that can be attained by carrier synchronizers. It turns out that the Cramér-Rao bounds (*CRB*s) for joint estimations are functions of the location of the reference symbols in the burst. The issue to find the optimal burst format that minimizes the frequency *CRB* has been already addressed in

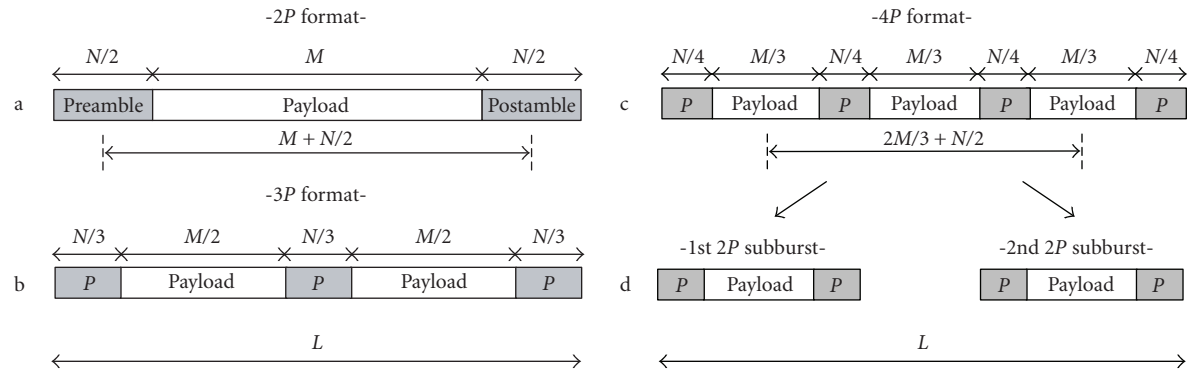

FIGURE 1: 2*P* burst format, 3*P* burst format, and 4*P* burst format.

[12–14], but only for joint carrier phase/Doppler-shift estimation. The novelty of the paper is to extend the analysis to the joint carrier phase/Doppler-shift *and* Doppler-rate estimation. It is known [12–15] that the preamble-postamble format (2*P* format) described in the sequel minimizes the frequency *CRB* with no Doppler-rate, and with constraints on the total training block length and on the burst overhead of the signal. We demonstrate here that such format is optimal in the presence of Doppler-rate as well, and that the Doppler-rate *CRB* is minimized by estimation over three equal-length blocks of reference symbols that are equally spaced by data symbols (3*P* format). We also show that other formats are very close to optimality (4*P* format).

In addition to computation of the burst, we also introduce new high-resolution and low-complexity carrier Doppler-shift and Doppler-rate DA estimation algorithms for such optimal burst formats.

The paper is organized as follows. In Section 2, we first outline the received signal model affected by Doppler distortions. Next, in Section 3 we present and analyze a low-complexity DA Doppler-shift estimator for the optimal 2*P* format. Extensions of this algorithm for joint carrier phase/Doppler-shift *and* Doppler-rate estimation for the 2*P* format, the 3*P* format, and the sub-optimum 4*P* format, are introduced in Sections 4 and 5, respectively. Finally, some conclusions are drawn in Section 6.

2. SIGNAL MODEL

In this paper, we take into consideration three different data burst formats as depicted in Figure 1.

In all cases, the total number of pilot symbols that are known to the receiver is equal to N, and the total length of the "data payload" fields that contain information symbols is equal to M. The formats differ for the specific pilots arrangement in two/three/four groups of $N/2$, $N/3$, $N/4$ consecutive pilot symbols equally spaced by data symbols. Hereafter we will address them as "2*P*," "3*P*," "4*P*" formats as in Figures 1(a), 1(b), 1(c), respectively. We denote also with $L = N + M$ the overall burst length, and with η the burst overhead, that is, the ratio between the total number of pilot symbols and the total number of symbols within the burst:

$$\eta = \frac{N}{L} = \frac{N}{N+M} = \frac{1}{1+M/N}. \tag{1}$$

We also assume BPSK/QPSK data modulation for the pilot fields, and additive white Gaussian noise (AWGN) channel with no multipath. Filtering is evenly split between transmitter and receiver, and the overall channel response is Nyquist. Timing recovery is ideal but the received signal is affected by time-varying Doppler distortion. Filtering the received waveform with a matched filter and sampling at symbol rate at the zero intersymbol interference instants yields the following discrete-time signal:

$$z(k) = c_k e^{j\varphi_k} + n(k), \quad k = -\frac{L-1}{2}, \ldots, 0, \ldots, \frac{L-1}{2}, \tag{2}$$

where

$$\varphi_k = \theta + 2\pi\nu kT + \pi\alpha k^2 T^2 \tag{3}$$

is the instantaneous carrier excess phase, $\{c_k\}$ are unit-energy (QPSK) data symbols and L (odd) is the observation (burst) length. Also, $1/T$ is the symbol rate, θ is the unknown initial carrier phase, ν is the constant unknown carrier frequency offset (Doppler-shift), and finally α is the constant unknown carrier frequency rate-of-change (Doppler-rate). For signal model (2) to be valid, we assumed that the value of the Doppler-shift ν is much smaller than the symbol rate, and that the value of the Doppler-rate α is much smaller than the square of the symbol rate. The noise $n(k)$ is a complex-valued zero-mean WGN process with independent components, each with variance $\sigma^2 = N_0/(2E_s)$, where E_s/N_0 represents the ratio between the received energy-per-symbol and the one-sided channel noise power spectral density.

Estimation of ν and α from the received signal $z(k)$ requires preliminary modulation removal from the pilot fields. Broadly speaking, it is customary to adopt BPSK or QPSK modulation for pilot fields, so that modulation removal is easily carried out by letting $r(k) = c_k^* z(k)$. The result is

$$r(k) = e^{j\varphi_k} + w(k), \quad k \in \mathcal{K} = \left\{ \bigcup N_{P_i} \right\}, \tag{4}$$

where $\mathcal{K}$ is the symmetric set of N time indices corresponding to pilot symbols, and $w(k) = c_k^* n(k)$ is statistically equivalent to $n(k)$. We explicitly mention here that we have chosen a symmetrical range $\mathcal{K}$ with respect to the middle of the burst since such arrangement decouples the estimation of some parameters, as discussed in [12] and in Appendix B. The signal $r(k)$ will be considered from now on as our observed signal that allows to carry out the carrier synchronization functions. We show in Appendix B that the burst formats in Figure 1 are optimum so far as the estimation of parameters ν and α is concerned. To keep complexity low, we will *not* take into consideration here "mixed," partially blind, methods to perform carrier synchronization that use *both* the known pilot symbols *and* all of the intermediate data symbols of the burst, like envisaged in [16] for the case of channel estimation.

3. DOPPLER-SHIFT ESTIMATOR: FEPE ALGORITHM

We momentarily neglect the effect of the Doppler-rate α in (4), to concentrate on the issue of Doppler-shift estimation only. Under such hypothesis, (4) can be rewritten as follows:

$$r(k) = e^{j(\theta+2\pi\nu kT)} + w(k), \quad k \in K. \tag{5}$$

The 2P format minimizes the *CRB* for Doppler-shift estimation for joint carrier phase/Doppler-shift estimation [12–15]. Conventional frequency offset estimators for consecutive signal samples [3] are not directly applicable to a burst format encompassing a preamble and a postamble. In addition, straightforward solution of a maximum-likelihood estimation problem for ν appears infeasible. We introduce thus a new low-complexity algorithm suitable for the estimation of the Doppler-shift ν in (4) with the burst format as above. The key idea of the 2P frequency estimator is really a naive one: we start by computing two phase estimates, the one on the preamble section, and the other on the postamble, using the standard low-complexity maximum-likelihood (ML) algorithm [17]:

$$\hat{\theta}_1 = \arg\left\{\sum_{k=-(N+M-1)/2}^{-(M-1)/2} r(k)\right\}, \qquad \hat{\theta}_2 = \arg\left\{\sum_{k=(M-1)/2}^{(N+M-1)/2} r(k)\right\}, \tag{6}$$

where $\arg\{\cdot\}$ denotes the phase of the complex-valued argument. Then we associate the two phase estimates to the two midpoints of the preamble and postamble sections, respectively, whose time distance is equal to $(M + N/2)T$ (Figure 1(a)). After this is done, we simply derive the frequency estimate as the slope of the line that connects the two points $(-(M-1)/2 - N/4, \hat{\theta}_1)$ and $((M-1)/2 + N/4, \hat{\theta}_2)$ on the (*time*, *phase*) plane:

$$\hat{\nu} = \frac{|\,|\hat{\theta}_2|_{2\pi} - |\hat{\theta}_1|_{2\pi}\,|_{2\pi}}{2\pi(M + N/2)T}. \tag{7}$$

This simple algorithm is known as *frequency estimation through phase estimation* (FEPE) [15]. The operator $|x|_{2\pi}$ returns the value of x modulo 2π, in order to avoid phase ambiguities, and is trivial to implement when operating with fixed-point arithmetic on a digital hardware. It is easy to verify that such estimator is independent of the particular initial phase θ, that vanishes when computing the phase difference at the numerator of (7). It is also clear that the operating range of the estimator is quite narrow. In order not to have estimation ambiguities, we have to ensure that $-\pi \le |\hat{\theta}_2|_{2\pi} - |\hat{\theta}_1|_{2\pi} < \pi$, and therefore the range is bounded to

$$|\nu| \le \frac{1}{2(M + N/2)T}. \tag{8}$$

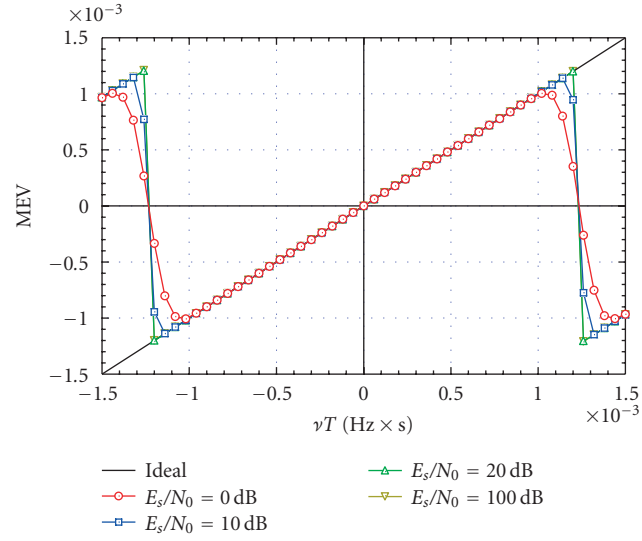

FIGURE 2: MEV of FEPE estimator for different values of E_S/N_0—simulation only. Preamble + postamble DA ML phase estimation, $N = 44$, $M = 385$.

This relatively narrow interval does not allow to use the FEPE algorithm for initial acquisition of a large frequency offset at receiver start-up. Its use is therefore restricted to fine estimation of a residual offset after a coarse acquisition or compensation of motion-induced Doppler-shift. Figure 2 depicts the normalized mean estimated value (MEV) curves of the FEPE algorithm (i.e., the average estimated value $E\{\hat{\nu}\}$ as a function of the true Doppler-shift ν) for different values of E_s/N_0 as derived by simulation. In our simulations we use the values $N = 44$ and $M = 385$ taken from the design described in [11], so that the overhead is $\eta = 10\%$ (typical for short bursts). MEV curves show that the algorithm is unbiased in a broad range around the true value (here, $\nu = 0$). It can be shown that this is true as long as $\nu 2NT \ll 1$, so that the "ancillary" estimates $\hat{\theta}_2$ and $\hat{\theta}_1$ are substantially unbiased as well. Such condition is implicitly assumed in (8) since in the practice $M \gg N/2$. The curve labeled $E_s/N_0 = 100$ dB (which is totally unrealistic) has the only purpose of showing the bounds of the unambiguous estimation range.

It is also easy to evaluate the estimation error variance of the FEPE estimator. It is known in fact that $\hat{\theta}_1$ and $\hat{\theta}_2$ in (7) have an estimation variance $\sigma^2_{\hat{\theta}}$ that achieves the Cramér-Rao

Bound (*CRB*) [17]:

$$\sigma^2_{\hat{\theta}} = \mathrm{CRB}(\theta) = \frac{1}{2 \cdot N/2} \frac{1}{E_s/N_0}. \tag{9}$$

Therefore, considering that the two phase estimates in (7) are independent, we get

$$\sigma^2_{\mathrm{FEPE}}(\hat{\nu}) = \frac{2 \cdot \sigma^2_{\hat{\theta}}}{4\pi^2(M+N/2)^2T^2} = \frac{1}{4\pi^2T^2N/2(M+N/2)^2} \frac{1}{E_s/N_0}. \tag{10}$$

The *vector CRB* [18] for the frequency offset estimate in the joint carrier phase/Doppler-shift estimation with the 2*P* format is derived in Appendix A and reads as follows:

$$\mathrm{VCRB}_{2P}(\nu) = \frac{3}{4\pi^2T^2(N/2)\left[4(N/2)^2+3M^2+3MN-1\right]} \frac{1}{E_s/N_0}. \tag{11}$$

Both from the expression of the bound (11) and of the variance (10), it is seen that the estimation accuracy has an inverse dependence on $(N/2)^3$, and this is nothing new with respect to conventional estimation on a preamble only. The important thing is that we also have inverse dependence on M^2, due to the 2*P* format that gives enhanced accuracy (with small estimation complexity) with respect to the conventional estimator. From (1), we also have $M = N(1/\eta - 1)$, so that the term $3M^2$ dominates $(N/2)^2$ as long as $\eta < 1/2$, which is always verified in the practice.

Therefore, the ratio between the CRB (11) and the variance of the FEPE estimator is very close to 1. With $N = 44$ and $M = 385$, we get, for instance, $\sigma^2_{\mathrm{FEPE}}/\mathrm{VCRB}_{2p} = 0.99$. The enhanced-accuracy feature is also apparent in the comparison of the $\mathrm{VCRB}_{2p}(\nu)$ as in (11) with the conventional $\mathrm{VCRB}(\nu)$ [18] for frequency estimation on a single preamble with length N, that is obtained by letting $M = 0$ in (11). The reverse of the coin is of course the reduced operating range (8) of the estimator.

Figure 3 shows curves of the (symbol-rate-normalized) RMSEE (root mean square estimation error) of the FEPE algorithm (i.e., $T\sqrt{E\{(\hat{\nu}-\nu)^2\}}$) as a function of E_s/N_0 for various values of the true offset ν. In particular, marks are simulation results for σ^2_{FEPE}, whilst the lowermost line is the $\mathrm{VCRB}_{2p}(\nu)$. We do not report the curve for (10) since it would be totally overlapped with (11).

Performance assessment of the FEPE estimator is concluded in Figure 4 with the evaluation of the sensitivity of the RMSEE to different values of an uncompensated Doppler-rate α. Just to have an idea of practical values of αT^2 to be encountered in practice, we mention that the largest Doppler-rates in LEO satellites are of the order of 200 Hz/s [1, 19] for a carrier frequency of 2.2 GHz, and assuming a symbol rate of 2 Mbaud, we end up with the value $\alpha T^2 = 5.10^{-11}$. From simulation results, we highlight that the performance of this algorithm is affected by α, but only in the case of a normalized Doppler-rate $\alpha T^2 \geq 10^{-7}$, that is larger than those that are found in the practice.

Finally, the complexity of the FEPE estimator with respect to conventional methods of frequency estimation [3, 13] is presented in Table 1. It is clear that the strength of the FEPE algorithm is its very low complexity as compared to conventional algorithms.

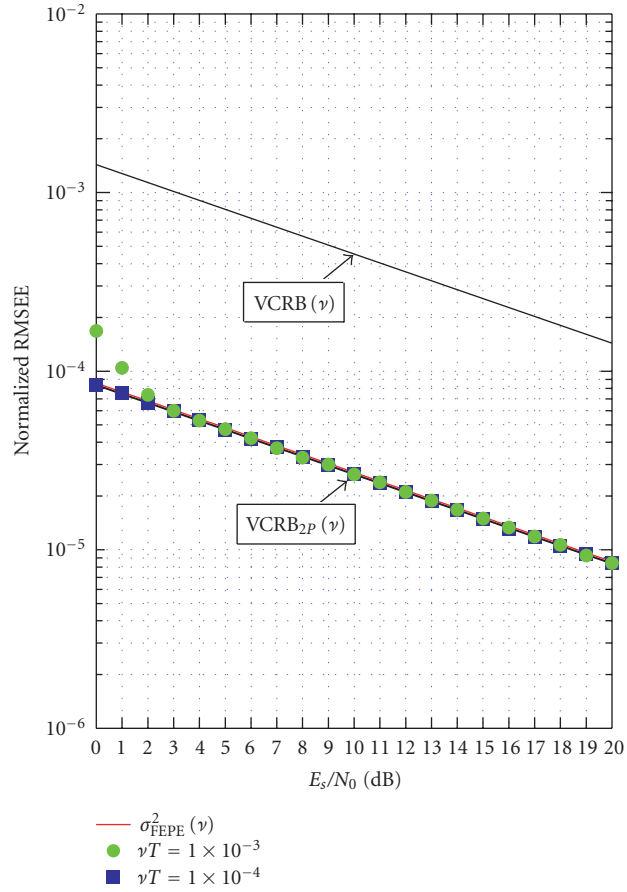

Figure 3: RMSEE of FEPE estimator for different values of E_S/N_0 and relevant bounds—solid lines: theory—marks: simulation. Preamble + postamble DA ML phase estimation, $N = 44$, $M = 385$.

4. DOPPLER-RATE ESTIMATORS IN 2*P* FRAME: FREPE AND FREFE ALGORITHMS

We take now back into consideration the presence of a non-negligible Doppler-rate in the received signal, modeled as in (3)-(4). We focus again on the 2*P* format (Figure 1(a)), since it is the optimal format for Doppler-shift estimation in joint carrier phase/Doppler-shift *and* Doppler-rate estimation too, as demonstrated in Appendix B. A new simple estimator for α in the 2*P* format is found by a straightforward generalization of the FEPE approach. Assume that we further split both the preamble and the postamble into two subsections of equal length, and we compute four (independent) ML phase estimates on the two subsections. We know in advance that the time evolution of the phase is described by a parabola. The four phase estimates can thus be used to fit a second-order phase polynomial according to the Minimum Mean Squared Error (MMSE) criterion; taking the origin in the

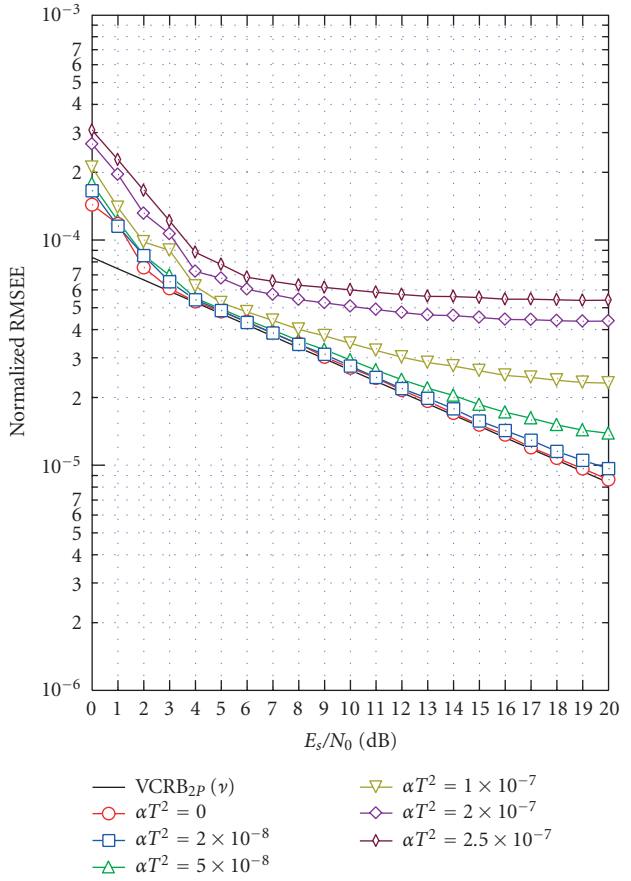

Figure 4: Sensitivity of FEPE estimator to different values of the Doppler-rate αT^2. Preamble + postamble DA ML phase estimation, $N = 44$, $M = 385$, $\nu T = 1.0 \times 10^{-3}$.

first section of the preamble, we obtain the phase model

$$\varphi_P(n) = a\pi\left(n + \frac{M-1}{2} + \frac{3N}{8}\right)^2 + 2\pi b\left(n + \frac{M-1}{2} + \frac{3N}{8}\right) + c, \tag{12}$$

where the regression coefficients a and b directly represent estimates for the (normalized) carrier Doppler-rate and Doppler-shift, respectively, and c is an estimate for the initial phase (that we are not interested into). The coefficients are found after observing that the MSE is written as

$$\varepsilon(a,b,c) = \sum_{i=1}^{4}\left[\varphi_P(n_i) - \hat{\theta}_i\right]^2 = \sum_{i=1}^{4} e_i^2, \tag{13}$$

where $\hat{\theta}_i$, $i = 1,\ldots,4$, are the above-mentioned ML phase estimates on $N/4$ pilots each, and $n_1 = -[(M-1)/2 + 3N/8]$, $n_2 = -[(M-1)/2 + N/8]$, $n_3 = [(M-1)/2 + N/8]$, and $n_4 = [(M-1)/2 + 3N/8]$ are the four time instants that we conventionally associate to the four estimates (the midpoints of the four subsections). Equating to zero the derivatives of

Table 1: The FEPE computational complexity comparison. (N_{alg} = estimation design parameter.)

Computational complexity of major Doppler-shift estimation algorithms			
Algorithm	*Reference*	*Number of real products and additions*	*LUT access*
L&R	[3]	$4N(N_{\text{alg}}+1)-2$	1
M&M	[3]	$N_{\text{alg}}(8N-4N_{\text{alg}}-3)-2$	N_{alg}
S-BLUE	[13]	$4N^2+4.5N-3$	$1.5N-2$
P-BLUE-2	[13]	$4N-1$	1
FEPE	—	$2N+3$	2

$\varepsilon(a,b,c)$ with respect to a, b, and c, we obtain

$$\begin{aligned}
\frac{\partial\varepsilon(a,b,c)}{\partial a} &= \sum_{i=1}^{4} e_i \cdot \left[n_i + \left(\frac{M-1}{2} + \frac{3N}{8}\right)\right]^2 = 0,\\
\frac{\partial\varepsilon(a,b,c)}{\partial b} &= \sum_{i=1}^{4} e_i \cdot \left[n_i + \left(\frac{M-1}{2} + \frac{3N}{8}\right)\right] = 0,\\
\frac{\partial\varepsilon(a,b,c)}{\partial c} &= \sum_{i=1}^{4} e_i = 0,
\end{aligned} \tag{14}$$

and solving for a we get the following so-called *frequency rate estimation through phase estimation* (FREPE) algorithm [15]:

$$\hat{\alpha}_{\text{FREPE}} = \frac{a}{T^2} = \frac{(\hat{\theta}_4 - \hat{\theta}_3) - (\hat{\theta}_2 - \hat{\theta}_1)}{\pi N/2(N/2+M)T^2} \tag{15}$$

(all differences to be intended modulo-2π). This extremely simple approach can be viewed as a generalization of the FEPE introduced in the previous section. In particular, by using (7), the terms

$$\frac{(\hat{\theta}_i - \hat{\theta}_{i-1})}{2\pi(N/4)T}, \quad i = 2,4, \tag{16}$$

represent two Doppler-shift estimations, the first on the preamble and the second on the postamble, respectively, which are spaced $M + N/2$ symbols apart. The Doppler-rate estimate is thus simply the difference between the two frequency estimates, divided by their time distance $(M+N/2)T$.

The considerations above allow us to also introduce the *frequency rate estimation through frequency estimation* (FREFE) algorithm [15]

$$\hat{\alpha}_{\text{FREFE}} = \frac{\hat{\nu}_2 - \hat{\nu}_1}{(M+N/2)T}, \tag{17}$$

wherein the two frequency estimates $\hat{\nu}_1$ and $\hat{\nu}_2$ can be obtained by any conventional algorithm [3] operating separately on the preamble and on the postamble, respectively. We can choose for instance the L&R algorithm [20] or the R&B algorithm [21]. Assuming that the selected algorithm operates close enough to the *CRB* (as is shown in [3]), the

variance of (17) is

$$\sigma^2_{\text{FREFE}}(\hat{\alpha}) = \frac{2\sigma^2_{\hat{\nu}}}{(M+N/2)^2T^2} = \frac{3}{\pi^2T^4N/2((N/2)^2-1)(M+N/2)^2}\frac{1}{E_s/N_0}, \tag{18}$$

where we have used $\sigma^2_{\hat{\nu}} = 3\cdot(E_s/N_0)^{-1}/[2\pi^2T^2N/2((N/2)^2-1)]$ [17]. This can be compared to the variance of the FREPE algorithm that is easily found to be

$$\sigma^2_{\text{FREPE}}(\hat{\alpha}) = \frac{4\cdot\sigma^2_{\hat{\theta}}}{\pi^2(N/2)^2(M+N/2)^2T^4} = \frac{4}{\pi^2T^4(N/2)^3(M+N/2)^2}\frac{1}{E_s/N_0}, \tag{19}$$

where now $\sigma^2_{\hat{\theta}} = (E_s/N_0)^{-1}/(N/2)$. The relevant vector *CRB* for Doppler-rate estimate is (see Appendix B):

$$\text{VCRB}_{2P}(\alpha) = \frac{45}{\pi^2T^4((N/2)^3-N/2)(16(N/2)^2+15M^2+30MN/2-4)}\frac{1}{E_s/N_0}. \tag{20}$$

All expressions inversely depend on $(N/2)^5$ as in conventional preamble-only estimation of the Doppler-rate [6], but they also bear again inverse dependence on M^2 that gives enhanced accuracy. For sufficiently large values of N and M, $M \gg N$, we have

$$\frac{\sigma^2_{\text{FREFE}}(\hat{\alpha})}{\sigma^2_{\text{FREPE}}(\hat{\alpha})} \cong \frac{3}{4}, \qquad \frac{\text{VCRB}_{PP}(\alpha)}{\sigma^2_{\text{FREFE}}(\hat{\alpha})} \cong 1. \tag{21}$$

Figure 5 shows the MEV curves (i.e., $E\{\hat{\alpha}\}$) of the FREPE algorithm for different values of E_s/N_0, in the case of $N = 44$, $M = 385$, and Doppler-shift $\nu T = 10^{-3}$. The estimator is unbiased with an operating range equal to

$$|\alpha_{\text{FREPE}}| \le \frac{1}{N/2(M+N/2)T^2}. \tag{22}$$

The sensitivity of FREPE to different uncompensated values of νT is illustrated in Figure 6 in terms of MEV.

The same simulations have been run also for the FREFE algorithm. In particular, Figure 7 illustrates the MEV curves for different values of E_s/N_0 and with $\nu T = 10^{-3}$. By using the L&R algorithm to estimate $\hat{\nu}_1$ and $\hat{\nu}_2$, the operating range of FREFE is roughly twice that of FREPE:

$$|\alpha_{\text{FREFE}}| \le \frac{1}{(N/4+1)(M+N/2)T^2}. \tag{23}$$

In particular, the term $[(N/2+1)T]^{-1}$ represents the frequency pull-in range of L&R on $N/2$ pilots [20].

Figure 8 demonstrates that FREPE is also less sensitive than FREFE to an uncompensated Doppler-shift. Finally, Figure 9 shows the curve of the Doppler-rate RMSEE of FREPE and FREFE as a function of E_s/N_0, for $\nu T = 10^{-3}$ and $\alpha T^2 = 10^{-6}$. The FREPE estimator loses only $10\log_{10}(4/3) = 1.25$ dB in terms of E_s/N_0 with respect to the performance of the more complex FREFE when $N \gg 1$.

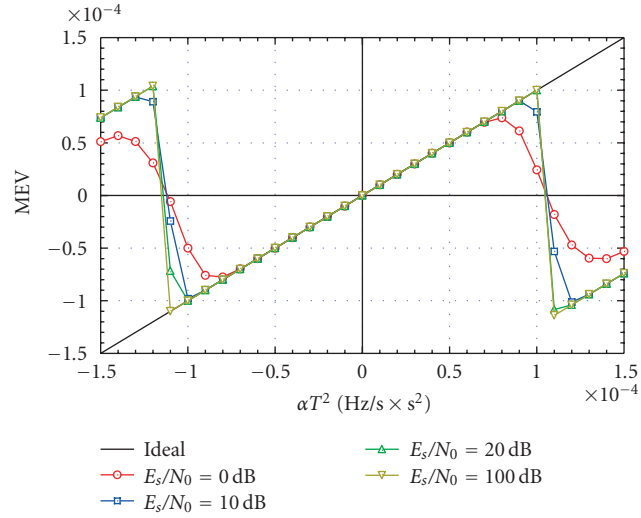

Figure 5: MEV of FREPE estimator for different values of E_S/N_0—simulation only. Preamble + postamble DA ML phase estimation, $N = 44$, $M = 385$, $\nu T = 1.0\times10^{-3}$.

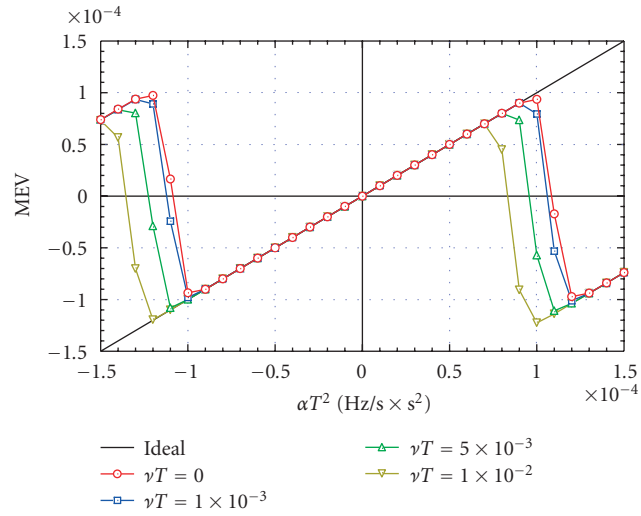

Figure 6: MEV of FREPE estimator for different values of the Doppler-shift νT—simulation only. Preamble + postamble DA ML phase estimation, $N = 44$, $M = 385$, $E_s/N_0 = 10$ dB.

5. OPTIMUM DOPPLER-RATE ESTIMATION

5.1. Odd number of pilot fields: FRE-3PE algorithm

We turn now to the issue of optimum burst configuration for the estimation of the Doppler-rate. We demonstrate in Appendix B that the 3*P* format (Figure 1(b)) minimizes the *CRB* for Doppler-rate estimation, with the usual constraints on the total training block length and on the burst overhead (1). In the following, we develop a new low-complexity algorithm suitable for Doppler-rate estimation with the 3*P* format. We know in advance that the time evolution of the phase is described by a parabola. As was done for the FREPE

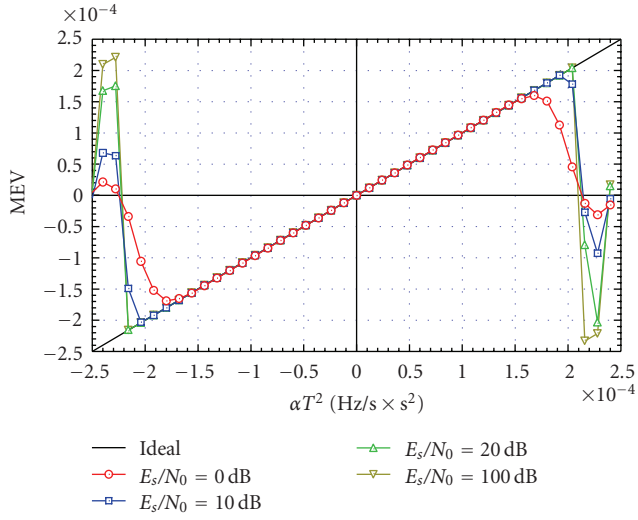

FIGURE 7: MEV of FREFE estimator for different values of E_S/N_0—simulation only. Preamble + postamble Luise and Reggiannini, $N = 44$, $M = 385$, $\nu T = 1.0 \times 10^{-3}$.

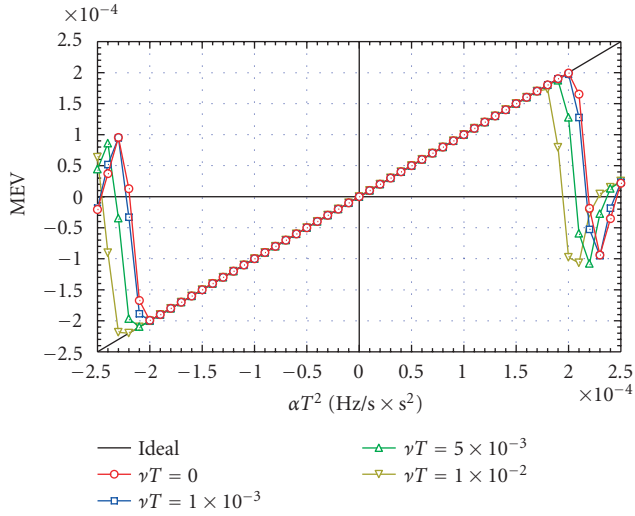

FIGURE 8: MEV of FREFE estimator for different values of the Doppler-shift νT—simulation only. FREFE estimator preamble + postamble Luise and Reggiannini, $N = 44$, $M = 385$, $E_s/N_0 = 10$ dB.

algorithm in the $2P$ configuration, a simple estimator of α in the $3P$ format is found by computing three (independent) ML phase estimates on the three blocks of pilots, and then fitting a second-order phase polynomial. Taking the origin in the first block of pilots, we obtain this time the phase model

$$\varphi_P(n) = a\pi\left(n + \frac{N}{3} + \frac{M}{2}\right)^2 + 2\pi b\left(n + \frac{N}{3} + \frac{M}{2}\right) + c. \quad (24)$$

The coefficients are found solving the following set of equations:

$$\varphi_P(n_i) = \hat{\theta}_i, \quad i = 1, \ldots, 3, \quad (25)$$

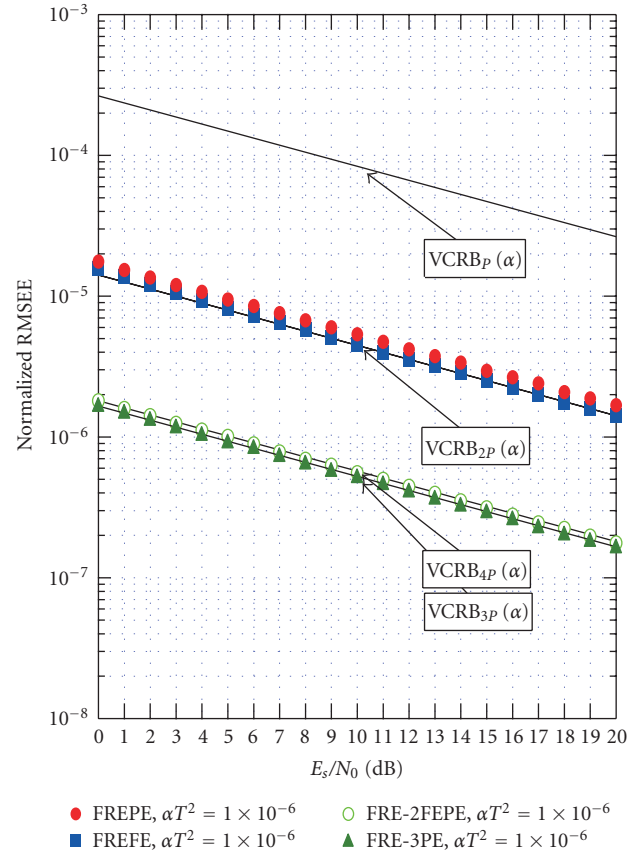

FIGURE 9: RMSEE of FREPE, FREFE, FRE-3PE, and FRE-2FREPE estimators for different values of E_S/N_0 and relevant bounds,—solid lines: theory—marks: simulation. Doppler-rate algorithms: FREFE versus FREPE versus FRE-3PE versus FRE-2FEPE, $N = 44(45)$, $M = 385(384)$, $\nu T = 1.0 \times 10^{-3}$.

where $\hat{\theta}_i$ are the above-mentioned ML phase estimates on $N/3$ pilots each, and where $n_1 = -(M/2 + N/3)$, $n_2 = 0$, and $n_3 = (M/2 + N/3)$ are the three time instants that we conventionally associate to the three estimates (the midpoints of the three subsections). Solving for a, we get the following so-called (FRE-3PE) (*frequency rate estimation through 3 phase estimations*) algorithm:

$$\hat{\alpha}_{\text{FRE-3PE}} = \frac{a}{T^2} = \frac{18[(\hat{\theta}_3 - \hat{\theta}_2) - (\hat{\theta}_2 - \hat{\theta}_1)]}{\pi(2N + 3M - 2)^2 T^2} \quad (26)$$

(all differences to be intended modulo-2π). The estimator is unbiased with an operating range equal to:

$$|\hat{\alpha}_{\text{FRE-3PE}}| \leq \frac{18}{(2N + 3M - 2)^2 T^2}. \quad (27)$$

In our simulations ($N = 45$ and $M = 384$), $|\alpha_{\text{FRE-3PE}} \cdot T^2| \leq 10^{-5}$. This range is narrower than FREPE's and FREFE's in the $2P$ format, but it still widely includes practical Doppler-rate values mentioned in Section 3. Figure 10 shows the MEV curves of the FRE-3PE algorithm for different values of E_s/N_0, in the case of $N = 45$, $M = 384$, and Doppler-shift

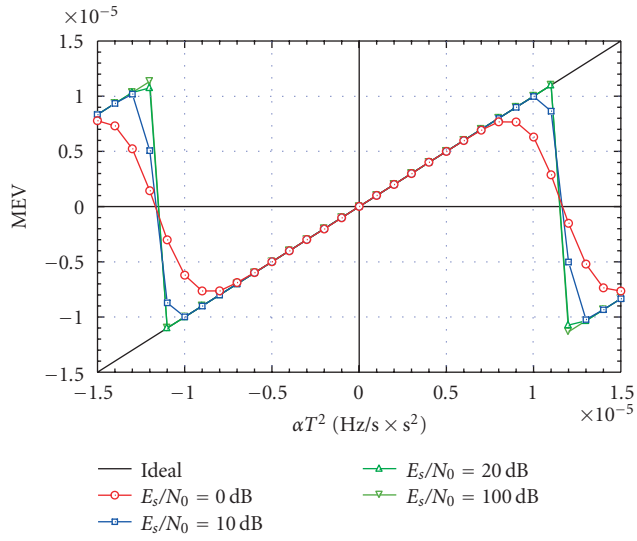

Figure 10: MEV of FRE-3PE estimator for different values of E_S/N_0—simulation only. 3 blocks of pilots DA ML phase estimation, $N = 45$, $M = 384$, $\nu T = 1.0 \times 10^{-3}$.

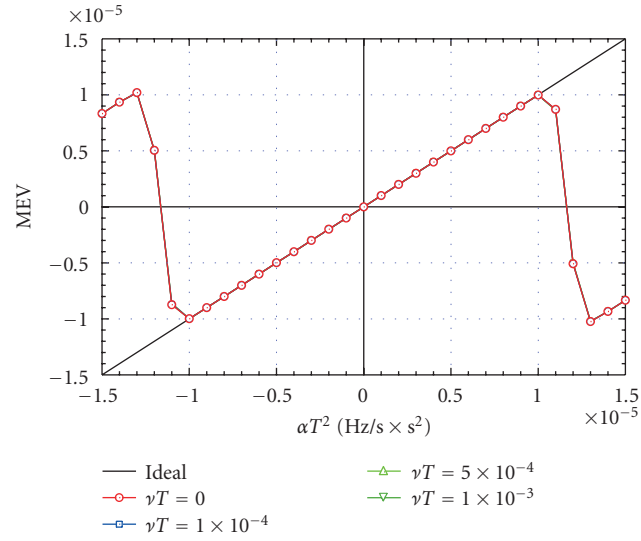

Figure 11: MEV of FRE-3PE estimator for different values of the Doppler-shift νT—simulation only. 3 blocks of pilots, $N = 45$, $M = 384$, $E_S/N_0 = 10$ dB.

$\nu T = 10^{-4}$, while Figure 11 shows the sensitivity of the MEV to different uncompensated values of the Doppler-shift νT.

The theoretical error variance of the FRE-3PE estimator can be easily evaluated, similarly to what was done for the calculation of $\sigma^2_{\text{FREFE}}(\hat{\alpha})$ in Section 4:

$$\sigma^2_{\text{FRE-3PE}}(\hat{\alpha}) = \frac{18^2 \cdot 6 \cdot \sigma^2_{\hat{\theta}}}{\pi^2(2N+3M-2)^4 T^4} = \frac{18^2 \cdot 6}{\pi^2 T^4 (2N/3)(2N+3M-2)^4} \frac{1}{E_s/N_0}, \tag{28}$$

where now $\sigma^2_{\hat{\theta}} = (E_s/N_0)^{-1}/(2N/3)$. Comparing this expression with the $\text{VCRB}_{3P}(\alpha)$ in (B.11) and with the variances of the FREFE and FREPE algorithms, we note that all expressions inversely depend on N^5 as in conventional preamble-only estimation of the Doppler-rate [6]. On the other hand, $\sigma^2_{\text{FRE-3PE}}(\hat{\alpha})$ and $\text{VCRB}_{3P}(\alpha)$ inversely depend on M^4, outperforming the accuracy of both the traditional preamble-only format and the $2P$ format (that depends on M^{-2}). The enhanced accuracy is highlighted by Figure 9, where we report the simulated RMSEE (marks) of FRE-3PE, FREPE, and FREFE versus E_s/N_0. To perform a fair comparison, we also reported the $\text{VCRB}_P(\beta)$, obtained in the case of estimation of Doppler-rate in the preamble-only configuration. The FRE-3PE algorithm attains its own CRB, and exhibits a gain of 19 dB in terms of E_s/N_0 with respect to the $2P$ format.

As a final remark, we only mention that a simple estimator of Doppler-shift in the $3P$ format is found by applying the FEPE algorithm to the two extreme pilot fields of the burst. Its variance reaches the $\text{VCRB}_{3P}(\nu)$ calculated setting $x = 1$ in (B.7) and (B.9), that is 1.5 dB apart from the $\text{VCRB}_{2P}(\nu)$ of the optimal $2P$ format.

5.2. Even number of pilot fields: FRE-2FEPE algorithm

When the number of pilot fields is even, the optimum burst format turns out to be the $4P$ as shown in Appendix B. We notice that the ratio of the two bounds for $3P$ and $4P$ amounts to $\text{VCRB}_{4p}(\alpha)/\text{VCRB}_{3p}(\alpha) \cong 9720/108 \cdot 640/51840 \cong 1.09$ $M \gg N$, so that $4P$ is only slightly optimal.

A simple estimator of α in the $4P$ format is found by a straightforward generalization of the FEPE and FREFE approaches. Assume that we split the burst into two $2P$ subbursts of length $(M/3 + N/2)$, (Figure 1(d)). Each preamble and postamble is now of length $N/4$, and we can derive two FEPE estimates of frequency on each subburst:

$$\hat{\nu}_1 = \frac{|\,|\hat{\theta}_2|_{2\pi} - |\hat{\theta}_1|_{2\pi}\,|_{2\pi}}{2\pi(M/3+N/4)T}, \qquad \hat{\nu}_2 = \frac{|\,|\hat{\theta}_4|_{2\pi} - |\hat{\theta}_3|_{2\pi}\,|_{2\pi}}{2\pi(M/3+N/4)T}, \tag{29}$$

where $\hat{\theta}_i$, $i = 1, \ldots, 4$, are the ML phase estimates computed on the four pilot fields of $N/4$ pilots each. The two Doppler-shift estimates $\hat{\nu}_1$ and $\hat{\nu}_2$ are associated with the two midpoint instants of the two $2P$ subbursts, whose time distance is equal to $(2M/3 + N/2)T$ (Figure 1(c)). Again, we estimate the Doppler-rate as the slope of the line that connects the two points $(-(M/3 - 1/2) - N/4, \hat{\nu}_1)$ and $((M/3 - 1/2) + N/4, \hat{\nu}_2)$ in the (*time*, *frequency*) plane:

$$\hat{\alpha}_{\text{FRE-2FEPE}} = \frac{\hat{\nu}_2 - \hat{\nu}_1}{(2M/3+N/2)T}. \tag{30}$$

We call this algorithm FRE-2FEPE (*frequency rate estimation through two FEPE estimations*) .

It is clear that the operating range of the estimator with respect to $\hat{\nu}$ comes from the application of (8) to the new configuration and turns out to be $|\nu| \leq [2(M/3+N/4)T]^{-1}$. The MEV curves of FRE-2FEPE are not reported here since

they basically mimic those in Figures 10 and 11 for the FRE-3PE algorithm. The estimation error variance of (30) is found to be

$$\sigma^2_{\text{FRE-2FEPE}}(\hat{\alpha}) = \frac{\sigma^2_{\hat{\theta}}}{(2M/3+N/2)^2(M/3+N/4)^2\pi^2T^2} = \frac{2\cdot(E_s/N_0)^{-1}}{\pi^2T^4N(2M/3+N/2)^2(M/3+N/4)^2}. \tag{31}$$

Figure 9 shows also the curves of the RMSEE of FRE-2FEPE and its respective *CRB*. The FRE-2FEPE algorithm reaches its own $\text{VCRB}_{4p}(\alpha)$ and thus, as demonstrated in Appendix B, it gains $10\log_{10}(7.19) = 18.5$ dB in terms of E_s/N_0 with respect to the performance of the previous algorithms with the 2*P* format. Also, the FRE-2FEPE loses only 0.4 dB with respect to the FRE-3PE algorithm and can thus be a valid alternative to the 3*P* format.

As a final remark, we briefly address the issue of Doppler-shift estimation in the 4*P* format. The best method is found by applying the FEPE algorithm to the two extreme pilot fields of the burst. Its variance is close to the $\text{VCRB}_{4P}(\nu)$ calculated setting $x = 1$ in (B.8) and (B.9), that is 2.4 dB worse than the $\text{VCRB}_{2P}(\nu)$ of the optimal 2*P* format.

6. CONCLUSIONS

In this paper, we presented and analyzed some very-low-complexity algorithms for carrier Doppler-shift and Doppler-rate estimation in burst digital transmission. To achieve enhanced accuracy, the burst configurations that minimize the *CRB* for the estimation of Doppler-shift and Doppler-rate are derived. Our analysis showed that the 2*P* format is optimum for Doppler-shift estimation and that the 3*P* format is optimum for Doppler-rate estimation. These two configurations can be practically thought as repetition of two/three consecutive conventional (preamble-only) bursts. Despite preventing from real-time processing of the data payload section, the 2*P* and 3*P* formats greatly outperform the estimation based on conventional preamble-only pilot distribution. Performance assessment has shown that all of the proposed algorithms are unbiased in practical operating conditions, and that their accuracy in terms of estimation variance gets remarkably close to their respective *CRB*s down to very low E_s/N_0 values.

APPENDICES

A. VCRB FOR JOINT CARRIER PHASE/DOPPLER-SHIFT ESTIMATION WITH 2*P* FORMAT

In this appendix, we calculate the *VCRB* for the error variance of any unbiased estimator of Doppler-shift in the case of joint estimation of phase/Doppler-shift using the preamble-postamble (2*P*) format. We explicitly mention that we have chosen a set $\mathcal{K}$ of pilot locations that is symmetrical with respect to the middle of the burst, since a symmetrical $\mathcal{K}$ decouples phase from Doppler-shift estimation, as discussed in [12]. After modulation removal, the generic sample within the preamble and the postamble is given by (5).

The Fisher information matrix (FIM) [18] can be written as

$$\mathbf{F} = \begin{bmatrix} F_{\theta\theta} & F_{\theta\nu} \\ F_{\nu\theta} & F_{\nu\nu} \end{bmatrix} = \begin{bmatrix} -E_{\underline{r}}\left\{\left|\dfrac{\partial^2 \ln p(\underline{r}\mid\widetilde{\nu},\widetilde{\theta})}{\partial\widetilde{\theta}^2}\right|\right\} & -E_{\underline{r}}\left\{\left|\dfrac{\partial^2 \ln p(\underline{r}\mid\widetilde{\nu},\widetilde{\theta})}{\partial\widetilde{\theta}\partial\widetilde{\nu}}\right|\right\} \\ -E_{\underline{r}}\left\{\left|\dfrac{\partial^2 \ln p(\underline{r}\mid\widetilde{\nu},\widetilde{\theta})}{\partial\widetilde{\nu}\partial\widetilde{\theta}}\right|\right\} & -E_{\underline{r}}\left\{\left|\dfrac{\partial^2 \ln p(\underline{r}\mid\widetilde{\nu},\widetilde{\theta})}{\partial\widetilde{\nu}^2}\right|\right\} \end{bmatrix}, \tag{A.1}$$

where $p(\underline{r}\mid\widetilde{\nu},\widetilde{\theta})$ is the probability density function of $\underline{r} = \{r(k)\}$, $k \in K$, conditioned on $(\widetilde{\nu},\widetilde{\theta})$, and $r(k)$ is a random Gaussian variable with variance equal to $\sigma^2 = N_0/(2E_s)$ and mean value equal to

$$\widetilde{s}(k) = e^{j(\widetilde{\theta}+2\pi\widetilde{\nu}kT)}. \tag{A.2}$$

Therefore, we write $p(\underline{r}\mid\widetilde{\nu},\widetilde{\theta})$ as

$$p(\underline{r}\mid\widetilde{\nu},\widetilde{\theta}) = \prod_{k\in K} p(r_k\mid\widetilde{\nu},\widetilde{\theta}) = \frac{1}{(2\pi\sigma^2)^N}\exp\left\{-\frac{1}{2\sigma^2}\sum_{k\in K}|r(k)-\widetilde{s}(k)|^2\right\}. \tag{A.3}$$

Taking the logarithm of (A.3), we obtain

$$\begin{aligned}\ln p(\underline{r}\mid\widetilde{\nu},\widetilde{\theta}) &= N\ln\left(\frac{1}{2\pi\sigma^2}\right) - \frac{1}{2\sigma^2}\sum_{k\in K}\left[|r(k)|^2 + |\widetilde{s}(k)|^2 - 2\text{Re}\{r(k)\widetilde{s}^*(k)\}\right] \\ &= C + \frac{1}{\sigma^2}\sum_{k\in K}\text{Re}\{r(k)\widetilde{s}^*(k)\},\end{aligned} \tag{A.4}$$

where C is a constant term that includes all the quantities independent of $\widetilde{\nu}$ and $\widetilde{\theta}$. After differentiating twice (A.4) with respect to $\widetilde{\nu}$ and $\widetilde{\theta}$, calculating the expectation of the various terms with respect to r, we get

$$\mathbf{F} = \begin{bmatrix} a' & b' \\ c' & d' \end{bmatrix}, \tag{A.5}$$

where

$$\begin{aligned} a' &= \left(\frac{1}{\sigma^2}\right)\sum_{k\in K}\{(1)E_{\underline{r}}[\text{Re}\{r(k)\widetilde{s}^*(k)\}]\}, \\ b' &= \left(\frac{1}{\sigma^2}\right)\sum_{k\in K}\{(2\pi Tk)E_{\underline{r}}[\text{Re}\{r(k)\widetilde{s}^*(k)\}]\}, \\ c' &= \left(\frac{1}{\sigma^2}\right)\sum_{k\in K}\{(2\pi Tk)E_{\underline{r}}[\text{Re}\{r(k)\widetilde{s}^*(k)\}]\}, \\ d' &= \left(\frac{1}{\sigma^2}\right)\sum_{k\in K}\{(4\pi^2T^2k^2)E_{\underline{r}}[\text{Re}\{r(k)\widetilde{s}^*(k)\}]\}. \end{aligned} \tag{A.6}$$

By noticing that

$$E_{\underline{r}}[\mathrm{Re}\{r(k)\widehat{s}^{*}(k)\}] = 1, \tag{A.7}$$

we obtain

$$\mathbf{F} = \frac{1}{\sigma^2}\begin{bmatrix} \sum_{k\in K}(1) & 2\pi T\sum_{k\in K}k \\ 2\pi T\sum_{k\in K}k & 4\pi^2T^2\sum_{k\in K}k^2 \end{bmatrix}, \tag{A.8}$$

where, considering the symmetry of the range $\mathcal{K}$,

$$\sum_{k\in K}(1) = N, \qquad \sum_{k\in K}k = 0, \tag{A.9}$$

$$\sum_{k\in K}k^2 = \frac{N/2}{3}\left[8\left(\frac{N}{2}\right)^2 - 6\left(\frac{N}{2}\right) + 1 + 3M^2 + 3M\left(3\left(\frac{N}{2}\right) - 1\right)\right]. \tag{A.10}$$

After calculation of $\mathbf{F}^{-1}$, the *VCRB* for ν in case of joint phase/Doppler-shift estimation is found to be

$$F^{-1}_{\nu\nu} = \mathrm{VCRB}_{2P}(\nu) = \frac{1}{2\pi^2T^2\sum_{k\in K}k^2}\frac{1}{E_s/N_0} = \frac{3\cdot(E_s/N_0)^{-1}}{4\pi^2T^2(N/2)[4(N/2)^2+3M^2+3MN-1]}. \tag{A.11}$$

B. OPTIMAL SYMMETRIC BURST CONFIGURATION FOR JOINT CARRIER-PHASE/DOPPLER-SHIFT AND DOPPLER-RATE ESTIMATION: 2P, 3P, 4P FORMATS

This appendix addresses the optimal signal design for Doppler-shift ν and Doppler-rate α estimation in the case of joint phase/Doppler-shift *and* Doppler-rate estimation when the received signal is expressed by (2)–(4). The optimal training signal structure is developed by minimizing the vector Cramér-Rao bounds (*VCRB*s) [17, 18] for ν and α, with constraints on the total training block length and on the burst overhead (1) of the signal (4). In fact, the Cramér-Rao bounds (*CRB*s) for joint estimations are functions of the location of the reference symbols in the burst.

The issue of finding the optimal burst format that minimizes the frequency *CRB* has been already addressed in [12–14], but only for joint phase/Doppler-shift estimation. We restrict our analysis to a symmetric burst format. In the sequel, we demonstrate that this symmetry also decouples the estimation of Doppler-shift *and* Doppler-rate. Our attention is focused on a generic burst format as in Figure 12, either with an even (Figure 12(a)) or an odd (Figure 12(b)) number of blocks of pilots. Just to rehearse notation, we mention that the length of the burst is L symbols, N is the total number of pilot symbols, N_P is the number of reference symbols in each subgroup, M is the total number of data symbols, and M_D is the number of data symbols in each subgroup. In Figure 12(a), $2x_{\mathrm{even}}$ is the (even) number of subgroups of pilot symbols, and $(2x_{\mathrm{even}}+1)$ is the (odd) number of subgroups of data symbols; in Figure 12(b), $(2x_{\mathrm{odd}}+1)$ is the (odd) number of subgroups of pilot symbols, and $2x_{\mathrm{odd}}$ is the (even) number of subgroups of data symbols. In the sequel we find the values of x that minimize the *VCRB*s of ν and α, for fixed values of L, N, and M.

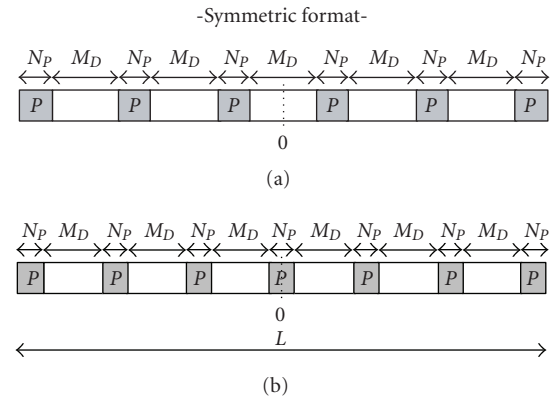

Figure 12: Generic symmetric burst format.

In the case of joint phase/Doppler-shift/Doppler-rate estimation, the fisher information matrix (FIM) of the generic bursts of Figure 12 can be written as

$$\mathbf{F} = \begin{bmatrix} F_{\theta\theta} & F_{\theta\nu} & F_{\theta\alpha} \\ F_{\nu\theta} & F_{\nu\nu} & F_{\nu\alpha} \\ F_{\alpha\theta} & F_{\alpha\nu} & F_{\alpha\alpha} \end{bmatrix} = \begin{bmatrix} -E_{\underline{r}}\left\{\left|\frac{a''}{\partial\widetilde{\theta}^2}\right|\right\} & -E_{\underline{r}}\left\{\left|\frac{a''}{\partial\widetilde{\theta}\partial\widetilde{\nu}}\right|\right\} & -E_{\underline{r}}\left\{\left|\frac{a''}{\partial\widetilde{\theta}\partial\widetilde{\alpha}}\right|\right\} \\ -E_{\underline{r}}\left\{\left|\frac{a''}{\partial\widetilde{\nu}\partial\widetilde{\theta}}\right|\right\} & -E_{\underline{r}}\left\{\left|\frac{a''}{\partial\widetilde{\nu}^2}\right|\right\} & -E_{\underline{r}}\left\{\left|\frac{a''}{\partial\widetilde{\nu}\partial\widetilde{\alpha}}\right|\right\} \\ -E_{\underline{r}}\left\{\left|\frac{a''}{\partial\widetilde{\alpha}\partial\widetilde{\theta}}\right|\right\} & -E_{\underline{r}}\left\{\left|\frac{a''}{\partial\widetilde{\alpha}\partial\widetilde{\nu}}\right|\right\} & -E_{\underline{r}}\left\{\left|\frac{a''}{\partial\widetilde{\alpha}^2}\right|\right\} \end{bmatrix}, \tag{B.1}$$

where $a'' = \partial^2 \ln p(\underline{r} \mid \widetilde{\alpha}, \widetilde{\nu}, \widetilde{\theta})$, $p(\underline{r} \mid \widetilde{\alpha}, \widetilde{\nu}, \widetilde{\theta})$ is the probability density function of $\underline{r} = \{r(k)\}$, with $k \in \mathcal{K}$, conditioned on $(\widetilde{\alpha}, \widetilde{\nu}, \widetilde{\theta})$. Now $r(k)$ is a random Gaussian variable with variance equal to $\sigma^2 = N_0/(2E_s)$ and mean equal to

$$\widetilde{s}(k) = e^{j(\widetilde{\theta}+2\pi\widetilde{\nu}kT+\widetilde{\alpha}\pi k^2T^2)} \tag{B.2}$$

so that

$$p(\underline{r} \mid \widetilde{\alpha}, \widetilde{\nu}, \widetilde{\theta}) = \prod_{k\in K} p(r_k \mid \widetilde{\alpha}, \widetilde{\nu}, \widetilde{\theta}) = \frac{1}{(2\pi\sigma^2)^N}\exp\left\{-\frac{1}{2\sigma^2}\sum_{k\in K}|r(k)-\widetilde{s}(k)|^2\right\}. \tag{B.3}$$

As detailed in Appendix A, after taking the logarithm of (B.3), and after differentiating with respect to the unknown parameters, and calculating the expectation of the terms with

respect to $\underline{r}$, we have

$$\mathbf{F} = \frac{1}{\sigma^2}\begin{bmatrix} \sum_{k\in K}(1) & 2\pi T\sum_{k\in K}k & \pi T^2\sum_{k\in K}k^2 \\ 2\pi T\sum_{k\in K}k & 4\pi^2T^2\sum_{k\in K}k^2 & 2\pi^2T^3\sum_{k\in K}k^3 \\ \pi T^2\sum_{k\in K}k^2 & 2\pi^2T^3\sum_{k\in K}k^3 & \pi^2T^4\sum_{k\in K}k^4 \end{bmatrix}, \quad \text{(B.4)}$$

where, thanks to the symmetry of range $\mathcal{K}$,

$$\sum_{k\in K}k = 0, \qquad \sum_{k\in K}k^3 = 0. \quad \text{(B.5)}$$

We finally get the expression of the FIM matrix as

$$\mathbf{F} = \frac{1}{\sigma^2}\begin{bmatrix} N & 0 & \pi T^2\sum_{k\in K}k^2 \\ 0 & 4\pi^2T^2\sum_{k\in K}k^2 & 0 \\ \pi T^2\sum_{k\in K}k^2 & 0 & \pi^2T^4\sum_{k\in K}k^4 \end{bmatrix}. \quad \text{(B.6)}$$

With an even number of pilot fields (Figure 12(a)), we have

$$\sum_{k\in K}k^2 = 2\sum_{n=0}^{x_{\text{even}}-1}\sum_{l=1}^{N/2x_{\text{even}}}\left[\frac{(M/(2x_{\text{even}}-1)-1)}{2} + l + \left(\frac{N}{2x_{\text{even}}} + \frac{M}{2x_{\text{even}}-1}\right)n\right]^2,$$
$$\sum_{k\in K}k^4 = 2\sum_{n=0}^{x_{\text{even}}-1}\sum_{l=1}^{N/2x_{\text{even}}}\left[\frac{(M/(2x_{\text{even}}-1)-1)}{2} + l + \left(\frac{N}{2x_{\text{even}}} + \frac{M}{2x_{\text{even}}-1}\right)n\right]^4 \quad \text{(B.7)}$$

while, with an odd number of pilot fields (Figure 12(b)), we get

$$\sum_{k\in K}k^2 = 2\sum_{k=1}^{N/(2x_{\text{odd}}+1)-1}k^2 + 2\sum_{n=0}^{x_{\text{odd}}-1}\sum_{l=1}^{N/(2x_{\text{odd}}+1)}\left[\frac{(N/(2x_{\text{odd}}+1)-1)}{2} + l + \left(\frac{N}{2x_{\text{odd}}} + \frac{M}{2x_{\text{odd}}+1}\right)n + \frac{M}{2x_{\text{odd}}}\right]^2,$$
$$\sum_{k\in K}k^4 = 2\sum_{k=1}^{N/(2x_{\text{odd}}+1)-1}k^4 + 2\sum_{n=0}^{x_{\text{odd}}-1}\sum_{l=1}^{N/(2x_{\text{odd}}+1)}\left[\frac{(N/(2x_{\text{odd}}+1)-1)}{2} + l + \left(\frac{N}{2x_{\text{odd}}} + \frac{M}{2x_{\text{odd}}+1}\right)n + \frac{M}{2x_{\text{odd}}}\right]^4. \quad \text{(B.8)}$$

Note that, thanks to the symmetry of the burst, the elements $F_{\theta\nu}$, $F_{\nu\theta}$, $F_{\alpha\nu}$, $F_{\nu\alpha}$ are all zero, which means that the joint phase/Doppler-shift and Doppler-shift/Doppler-rate estimations are decoupled.

Calculating $\mathbf{F}^{-1}$, we obtain the *VCRB*s for the estimation of ν as follows:

$$F^{-1}_{\nu\nu} = \text{VCRB}(\nu) = \frac{1}{2\pi^2T^2\sum_{k\in K}k^2}\frac{1}{E_s/N_0}, \quad \text{(B.9)}$$

as the one found in (A.11) without any Doppler-rate. The optimal burst configuration that minimizes the *VCRB* for ν is thus the $2P$ format found in [14] also in the presence of Doppler-rate effects.

The *VCRB* for α is

$$F^{-1}_{\alpha\alpha} = \text{VCRB}(\alpha) = -\frac{2N}{\pi^2T^4\left[\left(\sum_{k\in K}k^2\right)^2 - N\sum_{k\in K}k^4\right]}\frac{1}{E_s/N_0}. \quad \text{(B.10)}$$

If we compute $F^{-1}_{\alpha\alpha}$ as a function of x through (B.7) and (B.8), for both configurations of Figure 12, we find that the minimum for $F^{-1}_{\alpha\alpha}$ is obtained with $x_{\text{odd}} = 1$ in (B.8). This was found by exhaustive numerical evaluation with practical values for M and N. We can conclude that the *VCRB* of the error variance of any unbiased estimator of α is always minimized for a configuration with three blocks of pilot symbols equally spaced by two blocks of data symbols ($3P$ format). Setting $x_{\text{odd}} = 1$ in (B.8) and (B.10), the minimum VCRB of the error variance of any unbiased estimator of α for the optimal $3P$ format is thus

$$\begin{aligned}\text{VCRB}_{\min}(\alpha) &= F^{-1}_{\alpha\alpha}\big|_{x_{\text{odd}}=1} = \text{VCRB}_{3P}(\alpha) \\ &= 9720\cdot(E_s/N_0)^{-1}/(\pi^2T^4N[108(4-5N^2+N^4) \\ &\quad + 32MN(15N^2-45) \\ &\quad + 24M^2(35N^2-45) \\ &\quad + 720NM^3 + 270M^4]).\end{aligned} \quad \text{(B.11)}$$

In order to evaluate the gain in using the $3P$ format, we have compared the $\text{VCRB}_{3P}(\alpha)$ to the bounds for α in other configurations. Figure 13 shows the ratios $\text{VCRB}_{2P}(\alpha)/\text{VCRB}_{3P}(\alpha)$, $\text{VCRB}_{4P}(\alpha)/\text{VCRB}_{3P}(\alpha)$, and $\text{VCRB}_{2P}(\alpha)/\text{VCRB}_{4P}(\alpha)$ as functions of the total number N of pilots and with $\eta = 10\%$. It is clear that for practical values of $N = 40 \div 70$, the $3P$ format exhibits a gain of $10\log(78.6) = 19$ dB in terms of E_s/N_0 with respect to the $2P$ format and of $10\log(1.1) = 0.4$ dB with respect to the $4P$ format. The accuracy of the $3P$ format and of the $4P$ format can be thus considered almost equivalent.

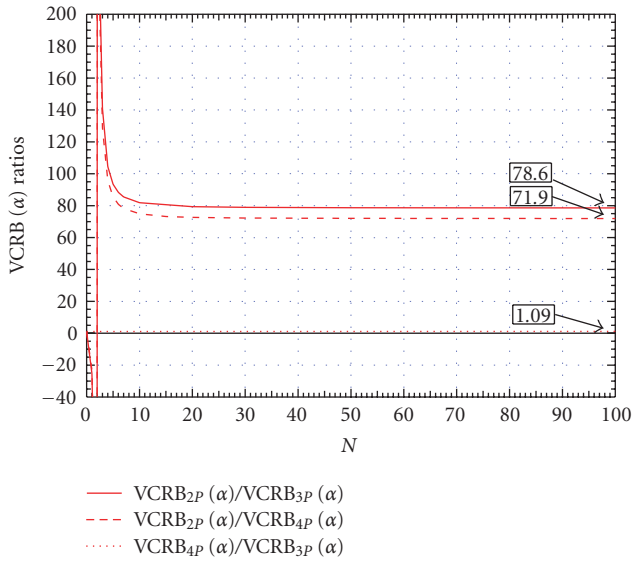

FIGURE 13: $\mathrm{VCRB}_{2P}(\alpha)/\mathrm{VCRB}_{3P}(\alpha)$, $\mathrm{VCRB}_{2P}(\alpha)/\mathrm{VCRB}_{4P}(\alpha)$ and $\mathrm{VCRB}_{4P}(\alpha)/\mathrm{VCRB}_{3P}(\alpha)$ ratios as function of the total number of pilots N.

The various *VCRB*s can be easily calculated from (B.10) using the appropriate x and (B.7) and (B.8). We report here the final expressions

$$\begin{aligned}\mathrm{VCRB}_{2P}(\alpha) &= F_{\alpha\alpha}^{-1}\big|_{x_{\mathrm{even}}=1} \\ &= \frac{360\cdot\left(E_s/N_0\right)^{-1}}{\pi^2T^4\left(N^3-4N\right)\left(4N^2+15M^2+15MN-4\right)},\end{aligned} \tag{B.12}$$

$$\begin{aligned}\mathrm{VCRB}_{4P}(\alpha) &= F_{\alpha\alpha}^{-1}\big|_{x_{\mathrm{odd}}=2} \\ &= 25920\cdot\left(E_s/N_0\right)^{-1}/\left(\pi^2T^4N\left(288N^4+1305N^3M\right.\right. \\ &\quad +240NM\left(8M^2-15\right) \\ &\quad +30N^2\left(77M^2-48\right) \\ &\quad \left.\left.+32\left(20M^4-75M^2+36\right)\right)\right).\end{aligned} \tag{B.13}$$

REFERENCES

[1] I. Ali, N. Al-Dhahir, and J. E. Hershey, "Doppler characterization for LEO satellites," *IEEE Transactions on Communications*, vol. 46, no. 3, pp. 309–313, 1998.

[2] "Special Issue on communications in the intelligence transportation system," *IEEE Communications Magazine*, vol. 34, 1996.

[3] M. Morelli and U. Mengali, "Feedforward frequency estimation for PSK: a tutorial review," *European Transactions on Telecommunications*, vol. 9, no. 2, pp. 103–116, 1998.

[4] F. Giannetti, M. Luise, and R. Reggiannini, "Simple carrier frequency rate-of-change estimators," *IEEE Transactions on Communications*, vol. 47, no. 9, pp. 1310–1314, 1999.

[5] M. Morelli, "Doppler-rate estimation for burst digital transmission," *IEEE Transactions on Communications*, vol. 50, no. 5, pp. 707–710, 2002.

[6] P. M. Baggenstoss and S. M. Kay, "On estimating the angle parameters of an exponential signal at high SNR," *IEEE Transactions on Signal Processing*, vol. 39, no. 5, pp. 1203–1205, 1991.

[7] T. J. Abatzoglou, "Fast maximum likelihood joint estimation of frequency and frequency rate," *IEEE Transactions on Aerospace and Electronic Systems*, vol. 22, no. 6, pp. 708–715, 1986.

[8] T. S. Rappaport, *Wireless Communications: Principles & Practice*, Prentice-Hall, Englewood Cliffs, NJ, USA, 1999.

[9] J. A. Gansman, J. V. Krogmeier, and M. P. Fitz, "Single frequency estimation with non-uniform sampling," in *Proceedings of the 30th Asilomar Conference on Signals, Systems and Computers*, vol. 1, pp. 399–403, Pacific Grove, Calif, USA, November 1996.

[10] V. Lottici and M. Luise, "Embedding carrier phase recovery into iterative decoding of turbo-coded linear modulations," *IEEE Transactions on Communications*, vol. 52, no. 4, pp. 661–669, 2004.

[11] S. Benedetto, R. Garello, G. Montorsi, et al., "MHOMS: high-speed ACM modem for satellite applications," *IEEE Wireless Communications*, vol. 12, no. 2, pp. 66–77, 2005.

[12] F. Rice, "Carrier-phase and frequency-estimation bounds for transmissions with embedded reference symbols," *IEEE Transactions on Communications*, vol. 54, no. 2, pp. 221–225, 2006.

[13] H. Minn and S. Xing, "An optimal training signal structure for frequency-offset estimation," *IEEE Transactions on Communications*, vol. 53, no. 2, pp. 343–355, 2005.

[14] A. Adriaensen, A. Van Doninck, and W. Steinert, "MF-TDMA burst demodulatir design with pilot-symbol assisted frequency estimation," in *Proceedings of the 8th International Workshop on Signal Processing for Space Communications (SPSC '03)*, Catania, Italy, September 2003.

[15] L. Giugno and M. Luise, "Carrier frequency and frequency rate-of-change estimators with preamble-postamble pilot symbol distribution," in *Proceedings of IEEE International Conference on Communications (ICC '05)*, vol. 4, pp. 2478–2482, Seoul, Korea, May 2005.

[16] A. Zhuang and M. Renfors, "Combined pilot aided and decision directed channel estimation for the RAKE receiver," in *Proceedings of the 52nd IEEE Vehicular Technology Conference (VTC '00)*, vol. 2, pp. 710–713, Boston, Mass, USA, September 2000.

[17] U. Mengali and A. N. D'Andrea, *Synchronization Techniques for Digital Receivers*, Plenum Press, New York, NY, USA, 1997.

[18] F. Gini, R. Reggiannini, and U. Mengali, "The modified Cramér-Rao bound in vector parameter estimation," *IEEE Transactions on Communications*, vol. 46, no. 1, pp. 52–60, 1998.

[19] G. R. J. Povey and J. Talvitie, "Doppler compensation and code acquisition techniques for LEO satellite mobile radio communications," in *Proceedings of the 5th International Conference on Satellite Systems for Mobile Communications and Navigation*, pp. 16–19, London, UK, May 1996.

[20] M. Luise and P. Reggiannini, "Carrier frequency recovery in all-digital modems for burst-mode transmissions," *IEEE Transactions on Communications*, vol. 43, no. 2–4, pp. 1169–1178, 1995.

[21] D. C. Rife and R. R. Boorstyn, "Single-tone parameter estimation from discrete-time observations," *IEEE Transactions on Information Theory*, vol. 20, no. 5, pp. 591–598, 1974.